Exploring disordered quantum wires with non-equilibrium acoustic phonons

1996 J. Phys.: Condens. Matter 8 3121

(http://iopscience.iop.org/0953-8984/8/18/006)

J. Phys.: Condens. Matter **8** (1996) 3121–3138. Printed in the UK

Exploring disordered quantum wires with non-equilibrium acoustic phonons

M P Blencowe

The Blackett Laboratory, Imperial College, London SW7 2BZ, UK

Received 13 February 1996

Abstract. We examine the results of a recent experiment in which non-equilibrium acoustic phonons were used to probe an electron gas confined to a split-gate GaAs/AlGaAs quantum wire. The results showed a resistance decrease following the onset of the interaction between the confined electron gas and incident phonon beam and also peaks in resistance decrease versus gate voltage which approximately coincided with the conductance step edges. We obtain qualitative agreement with experiment using a model which assumes electron heating due to phonon absorption, together with a wire resistance temperature dependence arising from either (i) impurity scattering in the presence of electron–electron interactions, or (ii) weak localization with phase relaxation due to electron–electron scattering. Magnetoconductance measurements will be needed in order to determine which of these two gives the dominant temperature dependence. A third possible mechanism, the energy dependence of Coulomb scattering from remote donor impurities, gives rise to a resistance increase and is thus ruled out. Taking into account phonon focusing, we estimate the electron temperature increase for the heater geometry and heater temperature of the experiment and find that it is much smaller than the experimental estimate. Several possible explanations are given for this discrepancy.

1. Introduction

In a recent experiment [1], the interaction between an acoustic phonon beam and quantum wire electron gas was investigated for the first time. A split-gate GaAs/AlGaAs wire was used, with constantan film deposited on the back surface of the GaAs substrate directly opposite the wire generating the phonon beam when heated above the ambient temperature (see figure 1). The response of the electron gas was probed by measuring the change in wire resistance. Contrary to expectation, a *decrease* in resistance was observed with the onset of the interaction between the wire electrons and incident phonon beam. Furthermore, peaks in the resistance decrease were observed and these occured at approximately the same gate voltage values as for the conductance step edges.

From the observed resistance decrease we can immediately conclude that the electron–impurity backscattering rate (note forward scattering does not affect the wire resistance) must exceed the electron–phonon backscattering rate for the conditions of the experiment. There are four different electron–impurity scattering mechanisms which can give rise to a resistance decrease: (1) Coulomb scattering from remote donor impurities [2, 3], (2) impurity scattering in the presence of electron–electron interactions [4–6], (3) weak localization with phase relaxation governed by electron–electron scattering, (4) weak localization with phase relaxation governed by electron–phonon scattering (see, e.g., the review by Bergmann [7] and references therein).

0953-8984/96/183121+18$19.50

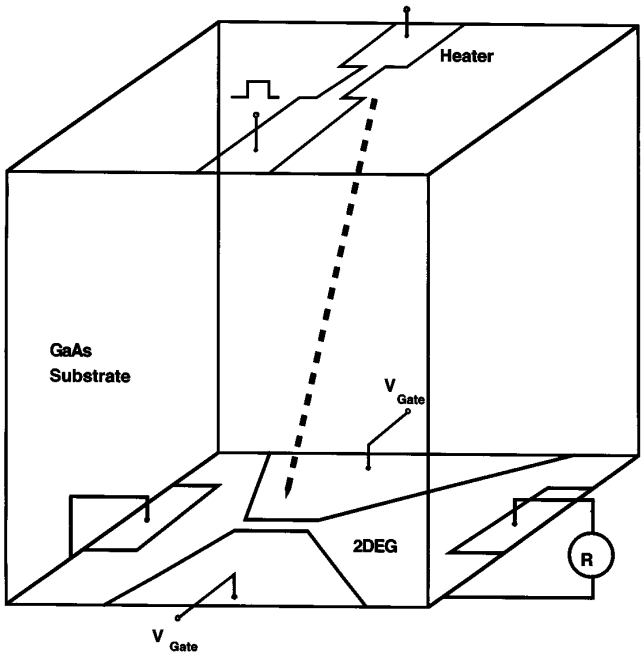

Figure 1. Schematic diagram of the experiment. See reference [1] for a detailed description.

Which of these mechanisms is the dominant cause for the resistance decrease depends, among other wire characteristics, on the electron–impurity backscattering length; weak (and strong) localization effects are expected to dominate when the backscattering length is much smaller than the wire length and also when the ambient and heater temperatures are sufficiently low. From the measured areal electron density (4.4×10^{15} m^{-2}) and mobility (100 m^2 V^{-1} s^{-1}) in the absence of an applied gate voltage, the transport length of the two-dimensional electron gas (2DEG) is determined to be about 10 μm—the same as the wire length. Thus, with the reduction in electron density and hence reduced screening of the remote donor impurities when the gate voltage is applied [8], it might be expected that the backscattering length of the confined electrons is smaller than the wire length. On the other hand, however, the quantum wire has far fewer states for the electrons at the Fermi level to backscatter into, than does the 2DEG and it is therefore possible that the backscattering length of the confined electrons exceeds the wire length [9].

Thus, it is not immediately obvious which of the above four mechanisms is the dominant cause. Further experiments to characterize the wire are required. For example, magnetoconductance measurements would be able to determine whether or not the resistance decrease is a weak localization effect [7]. Without the benefit of such experiments, however, it is necessary that we examine each of the four scattering mechanisms in turn. Weak localization with phase relaxation due to electron–phonon scattering has already been considered elsewhere [10], and so we will have little further to say about this mechanism in the present work. As we shall find out in the next section, scattering mechanisms (1)–(3) each give rise to qualitatively different resistance change versus gate voltage dependencies and, from a knowledge of the qualitative behaviour, we can almost certainly rule out Coulomb scattering from remote impurities as the dominant cause.

For scattering mechanisms (1)–(3), the resistance change results from a change in the

electron distribution. As a first approximation, the electrons are assumed to be in thermal equilibrium and absorption of phonons from the incident beam causes an increase in electron temperature. In section 3, we determine the magnitude of the electron temperature increase for the given heater geometry and other parameters of the experiment. We shall find that the calculated temperature increase is about two orders of magnitude smaller than the experimental value. We consider the various possible reasons for this discrepancy.

In common with the recent experiment, we restrict ourselves to the case where the heater is located directly opposite the wire. One of the advantages of non-equilibrium phonon experiments over simpler wire heating experiments is the possibility to obtain information concerning the phonon momentum angular dependence of the electron–phonon interaction. As we shall see in section 3, such information can be obtained by varying the heater dimensions. Of course, to obtain the most information concerning the angular dependence, the position of the heater with respect to the wire should be varied as well.

In the conclusion, we outline the main points of our analysis and suggest some possible extensions to the experiment in [1] in order to improve our understanding of the electron–phonon interaction in quantum wires. The appendix contains the technical details of the conductance calculations.

2. The scattering mechanisms

The gate voltage affects the wire conductance by changing both the Fermi level E_F and wire width [11, 12]. In the following subsections, we shall investigate the E_F dependence of the conductance change due to interaction with the incident phonon beam, keeping the wire width fixed. The wire width dependence is not expected to be qualitatively different from the E_F dependence. For each of the three scattering mechanisms, we shall be primarily concerned with the qualitative features of the conductance change versus E_F, in particular whether the change is positive and peaks close to a subband edge. In the final subsection we compare the E_F dependence of the conductance change for each of the three scattering mechanisms with that found in the experiment [1].

The conductance change is a consequence of the increase in electron temperature due to absorption of the non-equilibrium phonons. In the experiment, the electron temperature was estimated to increase by about a Kelvin (to within an order of magnitude) from an initial, ambient temperature of approximately 1 K. In the conductance change calculations, therefore, we choose as initial and final electron temperatures, 1 K and 2 K respectively. Discussion concerning the temperature increase is given in section 3.

2.1. Coulomb scattering from remote donor impurities

For the split-gate wire, we expect the electrons are predominantly scattered by the remote donor impurities, since scattering by the gate edge roughness is suppressed due to electrostatic smoothening of the roughness [13]. Assuming the donor impurities occupy a plane parallel to the 2DEG with separation h, the inverse of the elastic backscattering length for an electron with energy E initially in the Mth subband is approximately

$$l_M^{b-1}(E) \approx \frac{Z^2 e^4 m_*^2 \eta}{8\pi\hbar^4 \epsilon_0^2 \kappa_0^2} k_M^{-1}(E) \sum_N k_N^{-1}(E) \times \int_{-\infty}^{+\infty} \mathrm{d}q_x |Q_{MN}(q_x)|^2 \frac{\exp\left[-2h\sqrt{q_x^2 + (k_M(E) + k_N(E))^2}\right]}{\left[\sqrt{q_x^2 + (k_M(E) + k_N(E))^2} + q_s\right]^2} \quad (1)$$

where Ze is the impurity charge, η the areal impurity concentration, m_* the GaAs effective electron mass, κ_0 the GaAs static dielectric constant and $q_s = 2m_*e^2/(\overline{h}^2\kappa_0\epsilon_0)$ the 2D Thomas–Fermi screening wavevector. The wavevector k_M and function Q are defined as follows:

$$k_M(E) = \sqrt{\frac{2m_*}{\overline{h}^2}(E - E_M)} \tag{2}$$

$$Q_{MN}(q_x) := \int_{-\infty}^{+\infty} \mathrm{d}x \mathrm{e}^{\mathrm{i}q_x x} \chi_M^*(x)\chi_N(x) \tag{3}$$

where $\chi_M(x)$ is the transverse part of the electron energy eigenfunction for the ideal wire. We assume the transverse confining potential is approximately parabolic [11, 12] and therefore $\chi_M(x)$ is the energy eigenfunction of the harmonic oscillator with energy $E_M = (M+1/2)\overline{h}^2/(m_*w^2)$, $M = 0, 1, 2, \ldots$ where w is the effective wire width, estimated to be about 20 nm for the wire used in the experiment [1].

The Born approximation to the backscattering length, equation (1), is valid for E satisfying $E - E_M \gg \overline{h}/\tau_M(E)$, where τ_M is the scattering time. For the backscattering lengths we consider and for the above given wire width, there will be sufficient range of validity between subband edges to be able to obtain the relevant qualitative features of the conductance change.

In terms of the backscattering length (1), the wire conductance is (see the appendix for a derivation and also reference [14])

$$C \approx -\frac{2e^2}{\pi\overline{h}} \int \mathrm{d}E \frac{\partial}{\partial E}\left(\frac{1}{\mathrm{e}^{\beta(E-E_\mathrm{F})}+1}\right) \times \sum_{\substack{M \\ (E_M<E)}} \frac{l_M^\mathrm{b}(E)}{L}\left\{1 - \frac{l_M^\mathrm{b}(E)}{L}\left[1 - \exp\left(-\frac{L}{l_M^\mathrm{b}(E)}\right)\right]\right\} \tag{4}$$

where L is the wire length and $\beta^{-1} := k_\mathrm{B}T_\mathrm{e}$, with T_e the electron temperature. Notice that for $l_M^\mathrm{b} \ll L$, equation (4) gives the Drude conductance, while for the opposite regime $l_M^\mathrm{b} \gg L$, we recover the finite length, ideal wire conductance.

For $E_\mathrm{F} - E_M \gg k_\mathrm{B}T_\mathrm{e}$, we can expand (4) with respect to $k_\mathrm{B}T_\mathrm{e}$ to obtain the change in conductance due to the increase in electron temperature:

$$\Delta C \approx \frac{\pi e^2}{3\overline{h}} \sum_{\substack{M \\ (E_M<E_\mathrm{F})}} \frac{\partial^2}{\partial E^2}\left\{\frac{l_M^\mathrm{b}(E)}{L}\left[1 - \frac{l_M^\mathrm{b}(E)}{L}\left(1 - \exp\left(-\frac{L}{l_M^\mathrm{b}(E)}\right)\right)\right]\right\}_{E=E_\mathrm{F}} \times \left[(k_\mathrm{B}T_\mathrm{e}^\mathrm{f})^2 - (k_\mathrm{B}T_\mathrm{e}^\mathrm{i})^2\right] \tag{5}$$

where T_e^i and T_e^f are the initial and final electron temperatures, respectively. The sign of the conductance change ΔC is given by the sign of the second derivative with respect to E of the quantity in curly brackets. For the 2DEG, the corresponding quantity is $\tau(E)E$ which is proportional to E^γ with $2 < \gamma < 2.5$ for remote impurity scattering. Thus, if the mobility of the 2DEG is sufficiently low such that impurity scattering dominates phonon scattering, then an increase in mobility with increasing temperature will be observed [2, 3].

For the quantum wire, the conductance change behaviour is more complicated, a consequence of finite-size effects and intersubband scattering, neither of which are significant for the 2DEG. In figures 2 and 3, we show the E_F dependences of the $M = 1$ backscattering length and conductance change for a particular choice of scattering strength (i.e. impurity concentration η) and two different choices of electron gas-impurity layer separation h. In

figure 3, the E_F range starts just above the $M = 1$ subband edge and ends just below the $M = 2$ subband edge. Notice that there are regions of both positive and negative ΔC. Comparing the two figures, maximum positive ΔC occurs for $l^b_{M=1} \sim 0.1L$. A decrease in h causes a reduction in the maximum, demonstrating the importance of remote donors for positive ΔC. To the right of the maximum, ΔC decreases, eventually becoming negative when l^b_1 is comparable to or larger than L. To the left of the maximum, ΔC also becomes negative. This is due to intersubband scattering, since a calculation with intersubband scattering omitted is found to give positive ΔC.

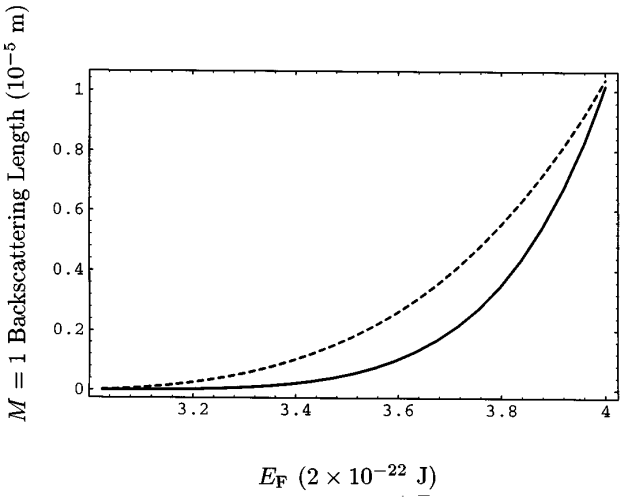

Figure 2. The $M = 1$ backscattering length versus E_F for different choices of electron gas-impurity layer separation h. The backscattering length is given in units of wire length $L = 10$ μm, while E_F is given in units of $\hbar^2/2m_*w^2 \approx 2 \times 10^{-22}$ J, so that $E_{M=1} = 3$ and $E_{M=2} = 5$. The solid line is for separation $h = 40$ nm, while the dashed line is for $h = 20$ nm.

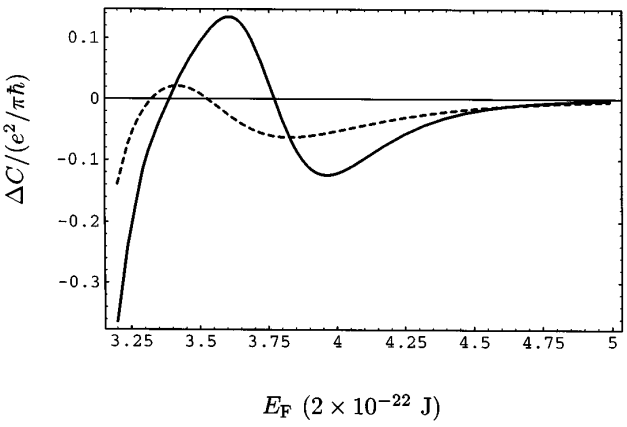

Figure 3. The conductance change versus E_F resulting from the temperature dependence of Coulomb scattering from remote donor impurities. The solid line is for $h = 40$ nm, while the dashed line is for $h = 20$ nm.

2.2. Impurity scattering in the presence of electron–electron interactions

Fukuyama and co-workers [4, 5] have carried out a theoretical investigation of the effect of the electron–electron interaction on the conductance of disordered quantum wires. The results of the recent wire heating experiments of Tarucha and co-workers [6] appear to support their theory. The electron–electron interaction gives rise to a temperature and length dependent correction to the backscattering length (1):

$$\tilde{l}_M^{\mathrm{b}-1}(E, T_{\mathrm{e}}, L) = l_M^{\mathrm{b}-1}(E) F_M(E, T_{\mathrm{e}}, L) \tag{6}$$

where

$$F_M(E, T_{\mathrm{e}}, L) \sim \left(\frac{\sqrt{(k_{\mathrm{B}} T_{\mathrm{e}})^2 + (\hbar^2 k_M(E)/(m_* L))^2}}{E - E_M} \right)^{K_\rho - 1}. \tag{7}$$

Notice that the temperature dependence weakens with decreasing wire length and for point contacts we would have vanishing temperature dependence. For $k_M^{-1} \sim w \sim 20$ nm and $T_{\mathrm{e}} \sim 1$ K, the temperature and length terms in (7) become comparable when $L \sim 1$ μm. Thus, for $L = 10$ μm, the length term in (7) can be neglected and we have strong temperature dependence. The exponent K_ρ is expected to be between 0.5 and 1 and therefore the backscattering length increases with increasing temperature. We shall choose the same value for K_ρ as that measured by Tarucha *et al* [6]: $K_\rho = 0.7$.

The conductance change ΔC resulting from the temperature dependence of the electron–electron correction term (7) is obtained by replacing l^{b} by $\tilde{l}^{\mathrm{b}}$ in the conductance formula (4) and setting $T_{\mathrm{e}} = 0$ in the Fermi distribution. In figure 4, we show the E_{F} dependence of ΔC for three different choices of scattering strength. The E_{F} range begins just above the $M = 1$ subband edge and ends just below the $M = 2$ subband edge. Notice that ΔC is positive. As E_{F} approaches the $M = 1$ subband edge from above, ΔC first increases and then decreases with the peak in ΔC shifting towards the subband edge the weaker the scattering strength.

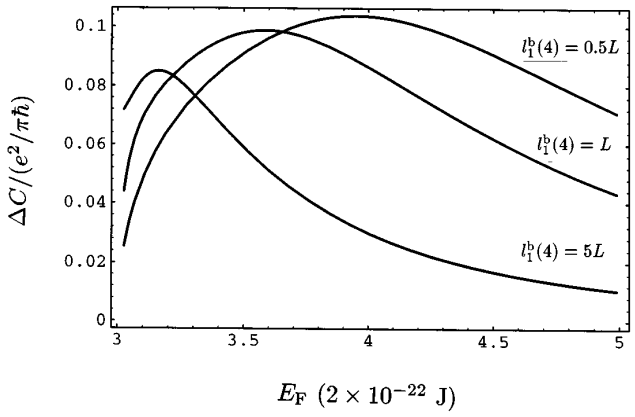

Figure 4. The conductance change versus E_{F} resulting from the temperature dependence of the electron–electron interaction correction to the elastic impurity backscattering length. The three different choices of scattering strength are identified by the value of $l_{M=1}^{\mathrm{b}}$ at $E_{\mathrm{F}} = 4$, half way between $E_1(= 3)$ and $E_2(= 5)$.

2.3. Weak localization with electron–electron phase relaxation

The weak localization contribution to the wire conductance is derived in the appendix. For E_F between the $M = 1$ and $M = 2$ subband edges, we have:

$$C_{wl} \approx -\frac{e^2}{\pi\hbar L}\left(\frac{\tau_{10}^{b-1}\tau_0^b v_0^2 + \tau_{01}^{b-1}\tau_1^b v_1^2}{\tau_{10}^{b-1}\tau_0^{\phi-1} + \tau_{01}^{b-1}\tau_1^{\phi-1}}\right)^{1/2}\Bigg|_{E=E_F} \tag{8}$$

where τ_{MN}^{b-1} denotes the individual backscattering rate into the Nth subband (i.e. $\tau_M^{b-1} = \sum_N \tau_{MN}^{b-1}$, with $\tau_M^{b-1} = l_M^{b-1}\hbar k_M/m_*$), $\tau_M^{\phi-1}$ is the phase relaxation rate (we consider the case where the phase relaxation length is smaller than the wire length) and $v_M = \hbar k_M/m_*$ is the velocity. The 'mixing' of the $M = 0, 1$ channels in (8) is a consequence of the non-negligible intersubband backscattering with l_M^b given by (1).

In an ideal, single band quantum wire, the combined constraints of energy and momentum conservation suppress electron–electron scattering. However, elastic scattering from imperfections such as the fluctuating remote impurity potential will relax momentum conservation, enabling electron–electron scattering to occur. Thus, which of the two inelastic processes governs phase relaxation—electron–electron or electron–phonon scattering—will depend on, among other things, how disordered the wire is. We will consider here the conductance change resulting from the temperature dependence of the electron–electron phase relaxation rate. A discussion of the conductance change due to electron–phonon scattering is given in reference [10].

Altshuler *et al* [15] (see also references therein) derive the electron–electron phase relaxation rate for a quasi-1D wire. Assuming their formula also applies (at least qualitatively) to a wire with only a few occupied subbands, we have

$$\tau_M^{\phi-1} \sim \left(\frac{\pi k_B T_e}{\hbar}\right)^{2/3}\tau_M^{b-1/3}. \tag{9}$$

Substituting (9) into (8), we obtain for the conductance change:

$$\Delta C \sim \frac{e^2}{(\pi^2\hbar)^{2/3}L}\left(\frac{\tau_{10}^{b-1}\tau_0^b v_0^2 + \tau_{01}^{b-1}\tau_1^b v_1^2}{\tau_{10}^{b-1}\tau_0^{b-1/3} + \tau_{01}^{b-1}\tau_1^{b-1/3}}\right)^{1/2}\left[(k_B T_e^i)^{-1/3} - (k_B T_e^f)^{-1/3}\right]\Bigg|_{E=E_F}. \tag{10}$$

The conductance change is clearly positive and decreases in magnitude as E_F approaches the $M = 1$ subband edge from above. This is due to increased scattering into the $M = 1$ subband. As E_F descends below the subband edge, the conductance change increases (before decreasing again), since scattering into the $M = 1$ subband is suppressed.

2.4. Comparison of the different mechanisms with experiment

In the experiment [1], a positive conductance change was measured. We can therefore confidently rule out Coulomb scattering from remote impurities as the dominant cause, since this mechanism gives rise to E_F regions of negative conductance change (figure 3).

The measured conductance change peaked for $E_F \sim E_M$. From figure 4, we see that impurity scattering in the presence of electron–electron interactions gives rise to a peak which occurs to the right of a given subband edge. On the other hand, for weak localization with electron–electron phase relaxation, the peak in the conductance change occurs to the left of a given subband edge (note that electron–phonon phase relaxation gives similar behaviour [10]). For both mechanisms, the weaker the scattering strength, the closer the peak is to the subband edge. With these qualitative comparisons alone and for the given accuracy of the experiment, however, it is not really possible to single out either of the

two mechanisms as the dominant cause for the observed conductance change behaviour. A magnetoconductance experiment is essential to distinguish the two.

3. Electron heating

In the previous section, we showed how an increase in T_e can give rise to a positive conductance change. If a separate calibration experiment is carried out in which the wire conductance is measured as a function of ambient temperature and gate voltage with the heater turned off, then the wire conductance can be used as a thermometer for the electron temperature. The dependence of T_e on the heater temperature, heater geometry and E_F gives direct information concerning the quantum wire electron–phonon interaction. A partial calibration for a few gate voltage values was in fact carried out [1]. At a heater temperature $T_h \approx 8.8$ K and for a particular choice of gate voltage, T_e was estimated to increase by about 2.5 K above the ambient temperature $T_a \approx 1.3$ K.

In order to properly determine the electron temperature increase, we must take into account phonon focusing effects. The heater film lies in a {100} plane of the GaAs substrate and the wire is located directly opposite the heater, so that it receives heater phonons with momenta within some solid angle centred about a ⟨100⟩ direction. However, there is strong focusing in ⟨100⟩ directions: the effective solid angle can be much larger than that set by the heater size and heater-wire distance.

We shall determine the electron temperature by requiring that the net power absorbed by the wire equal zero. The net absorbed power per unit wire length is approximately (see, e.g., references [16, 17])

$$\begin{aligned} P \approx \frac{8\pi}{L}\sum_{s,\boldsymbol{q}}\omega_s(\boldsymbol{q})\sum_{I,J,k}|M_{IJs}(\boldsymbol{q})|^2\,\delta\left(E_I+(k+q_y)^2/2m_*-E_J-k^2/2m_*-\hbar\omega_s(\boldsymbol{q})\right) \\ \times f\left(E_I+(k+q_y)^2/2m_*\right)\left[1-f\left(E_J+k^2/2m_*\right)\right] \\ \times\left[\rho_s(\boldsymbol{q})\mathrm{e}^{\hbar\omega_s(\boldsymbol{q})/k_BT_e}-(\rho_s(\boldsymbol{q})+1)\right] \end{aligned} \tag{11}$$

where the electron–phonon matrix element is

$$M_{IJs}(\boldsymbol{q}) = \left(\frac{\hbar}{2\rho\omega_s(\boldsymbol{q})\Omega}\right)^{1/2}\Xi_s(\boldsymbol{q})Z(q_z)Q_{IJ}(q_x). \tag{12}$$

In (11), the first sum is over the phonon wavevector $\boldsymbol{q}$ and the three phonon polarizations, $s = 0$ (longitudinal), 1 (slow transverse) and 2 (fast transverse). We choose coordinates such that the y-axis runs along the wire and the z-axis is normal to the 2DEG. We assume the wire is aligned in the [010] direction. The function $f(E)$ is the Fermi–Dirac distribution, $\omega_s(\boldsymbol{q})$ is the phonon frequency and $\rho_s(\boldsymbol{q})$ is the (non-equilibrium) phonon distribution. In (12), ρ is the GaAs mass density and $Z(q_z) = \int \mathrm{d}z\,\exp(\mathrm{i}q_z z)\psi_0^*(z)\psi_0(z)$ is the form factor involving the part of the electron wavefunction perpendicular to the 2DEG. The form factor Q is defined in (3).

The electron–phonon interaction is assumed to be the same as that for bulk GaAs:

$$\Xi_s(\boldsymbol{q}) = \mathrm{i}C\boldsymbol{q}\cdot\xi_s + \frac{2h_{14}e}{q^2}(q_xq_y\xi_{sz}+q_yq_z\xi_{sx}+q_zq_x\xi_{sy}) \tag{13}$$

where C and h_{14} are the GaAs deformation potential and piezoelectric coupling constants, respectively, and ξ_s is the $\boldsymbol{q}$-dependent phonon polarization vector. Differences between the electron–phonon interaction in a bulk wire and in the quantum wire are therefore of kinematic origin: the form factor Q limits the magnitude of the q_x wavevector component

of a phonon which can be absorbed or emitted by a wire electron to less than the inverse of the wire width w. The form factor Z similarly limits the magnitude of the q_z wavevector to less than the inverse of the 2DEG width. Furthermore, the combined constraints of energy conservation and momentum conservation along the direction of the wire severely limit the range of q_y components for which absorption and emission can occur.

Assuming the heater phonons traverse the heater-wire distance without scattering, the phonon distribution at the wire is

$$\rho_s(\boldsymbol{q}) = \Theta_s(\boldsymbol{q})\left(\mathrm{e}^{\hbar\omega_s(\boldsymbol{q})/k_\mathrm{B}T_\mathrm{h}} - 1\right)^{-1} + [1 - \Theta_s(\boldsymbol{q})]\left(\mathrm{e}^{\hbar\omega_s(\boldsymbol{q})/k_\mathrm{B}T_\mathrm{a}} - 1\right)^{-1}. \tag{14}$$

The stepfunction $\Theta_s(\boldsymbol{q})$ is equal to one (and zero otherwise) for all $\boldsymbol{q}$ such that the group velocity vector $\boldsymbol{v}_s(\boldsymbol{q})$ $(= \nabla_{\boldsymbol{q}}\omega_s(\boldsymbol{q}))$ with origin at the heater surface points towards the wire. In figure 5, we give the phonon wavevector angular ranges for heater dimensions $\Delta x \times \Delta y = 100\ \mu\mathrm{m} \times 10\ \mu\mathrm{m}$ and heater-wire distance $D = 380\ \mu\mathrm{m}$, the same as for the experiment [1]. Notice that for the transverse polarizations the angular range along the wire direction is several times larger than the range which is obtained with the elastic anisotropy neglected.

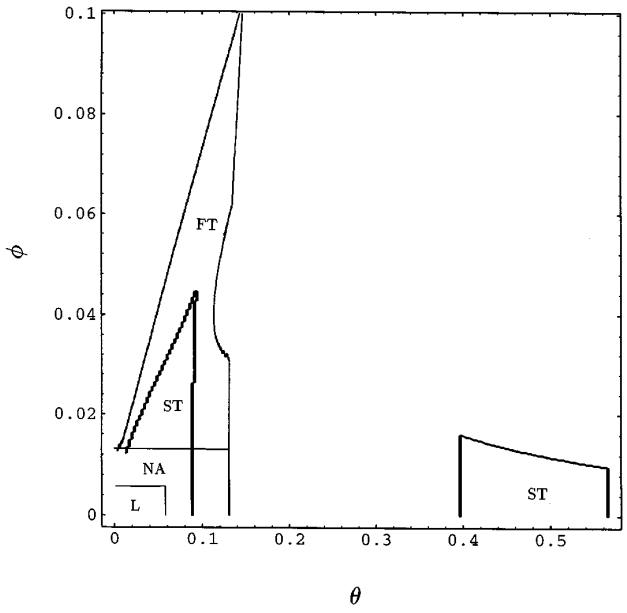

Figure 5. The boundaries of the phonon wavevector angular ranges for heater dimensions $\Delta x \times \Delta y = 100\ \mu\mathrm{m} \times 10\ \mu\mathrm{m}$ and heater–wire distance $D = 380\ \mu\mathrm{m}$. The ϕ angle is along the wire, while the θ angle is transverse to the wire. The angular coordinates are given in radians. Only one quadrant is indicated, the others obtained by reflecting about the θ and ϕ axes. The three phonon polarizations are: longitudinal (L), slow transverse (ST) and fast transverse (FT). The angular range neglecting elastic anisotropy (NA) is also given.

Summing over the electron wavevector k and simplifying the temperature-dependent terms, equation (11) becomes

$$P \approx \frac{m_*}{4\pi^3\rho\hbar}\sum_{I,J,s}\int \mathrm{d}\boldsymbol{q}|q_y|^{-1}|\Xi_s(\boldsymbol{q})Z(q_z)Q_{IJ}(q_x)|^2$$

$$\times\left[\left(\mathrm{e}^{(E_{IJs}(\boldsymbol{q})-E_{\mathrm{F}})/k_{\mathrm{B}}T_{\mathrm{e}}}+1\right)^{-1}-\left(\mathrm{e}^{(E_{IJs}(\boldsymbol{q})+\hbar\omega_s(\boldsymbol{q})-E_{\mathrm{F}})/k_{\mathrm{B}}T_{\mathrm{e}}}+1\right)^{-1}\right]$$
$$\times\left\{\left(\mathrm{e}^{\hbar\omega_s(\boldsymbol{q})/k_{\mathrm{B}}T_{\mathrm{a}}}-1\right)^{-1}-\left(\mathrm{e}^{\hbar\omega_s(\boldsymbol{q})/k_{\mathrm{B}}T_{\mathrm{e}}}-1\right)^{-1}\right.$$
$$\left.+\Theta_s(\boldsymbol{q})\left[\left(\mathrm{e}^{\hbar\omega_s(\boldsymbol{q})/k_{\mathrm{B}}T_{\mathrm{h}}}-1\right)^{-1}-\left(\mathrm{e}^{\hbar\omega_s(\boldsymbol{q})/k_{\mathrm{B}}T_{\mathrm{a}}}-1\right)^{-1}\right]\right\} \tag{15}$$

where

$$E_{IJs}(\boldsymbol{q}) := \frac{\hbar^2}{8m_*q_y^2}\left[q_y^2+\frac{2m_*}{\hbar^2}\left(\frac{\hbar^2}{m_*w^2}(I-J)-\hbar\omega_s(\boldsymbol{q})\right)\right]^2+\frac{\hbar^2}{m_*w^2}(J+\tfrac{1}{2}) \tag{16}$$

is the energy of an electron in the Jth subband which subsequently absorbs a phonon with wavevector $\boldsymbol{q}$ and scatters into the Ith subband. Notice that, once the phonon wavector $\boldsymbol{q}$ and subband labels I and J are given, the initial and final energies of the electron are completely fixed by energy and momentum conservation.

Examining the Bose–Einstein terms in equation (15), it is clear that for $T_{\mathrm{h}} = T_{\mathrm{a}}$, we must also have $T_{\mathrm{e}} = T_{\mathrm{a}}$ in order that $P = 0$. That is, when the heater is turned off, the electron gas remains at the ambient temperature. If we have $T_{\mathrm{h}} > T_{\mathrm{a}}$, i.e. heater turned on, then the term involving the step function is positive and thus we must have $T_{\mathrm{e}} > T_{\mathrm{a}}$ in order to cancel this term.

In figure 6, we give the E_{F} dependence of the net absorbed power per unit wire length for $T_{\mathrm{h}} = 8.8$ K and $T_{\mathrm{e}} = T_{\mathrm{a}} = 1.3$ K. In figure 7, we give the E_{F} dependence of the net emitted (= − net absorbed) power per unit wire length for $T_{\mathrm{h}} = T_{\mathrm{a}} = 1.3$ K and a selection of values $T_{\mathrm{e}} > T_{\mathrm{a}}$. Comparing the magnitudes of the curves in the two figures, we can see that the predicted T_{e} increase will be on the order of tens of mK, two orders of magnitude smaller than the experimental value.

The E_{F} dependences of the curves in figures 6 and 7 point towards the reason for the low predicted temperature increase. Because the density of states of an ideal 1D wire diverges at the subband edges, we expect the emitted and absorbed powers to peak at the subband edges [17]. This is clearly the case for the emitted power in figure 7, while there are no such peaks for the absorbed power in figure 6. To understand why this is so, let us determine the condition energy conservation and momentum conservation parallel to wire imposes on the phonon wavevector component q_y and frequency $\omega_s(\boldsymbol{q})$ in order to have absorption. For $T_{\mathrm{e}} \sim 1$ K and $w \approx 20$ nm, we have $k_{\mathrm{B}}T_{\mathrm{e}} \ll E_{M+1} - E_M$ and therefore, from the Fermi–Dirac terms in (15), we see that $\boldsymbol{q}$ must satisfy $E_{IJs}(\boldsymbol{q}) \approx E_{\mathrm{F}}$ for non-negligible absorption. Suppose $E_{\mathrm{F}} = E_J$ and consider intrasubband scattering, i.e. $I = J$. Then solving (16) for q_y in terms of $\omega_s(\boldsymbol{q})$, we obtain the following condition

$$q_y = \sqrt{\frac{2m_*\omega_s(\boldsymbol{q})}{\hbar}}. \tag{17}$$

Approximating $\omega_s(\boldsymbol{q})$ by cq, where c is the average phonon phase velocity and noting also from the Bose–Einstein terms in (15) that the dominant wavenumber q for heater phonons is roughly $k_{\mathrm{B}}T_{\mathrm{h}}/\hbar c$, condition (17) becomes:

$$\frac{q_y}{q} \sim \sqrt{\frac{m_*c^2}{k_{\mathrm{B}}T_{\mathrm{h}}}} \approx 0.1 \tag{18}$$

where we have used the values $c = 5 \times 10^3$ m s^{-1} and $T = 10$ K. Therefore, in order to have substantial absorption of heater phonons when E_F is at a subband edge, the effective angular range of phonon momenta along the the wire must be somewhat larger than 0.1.

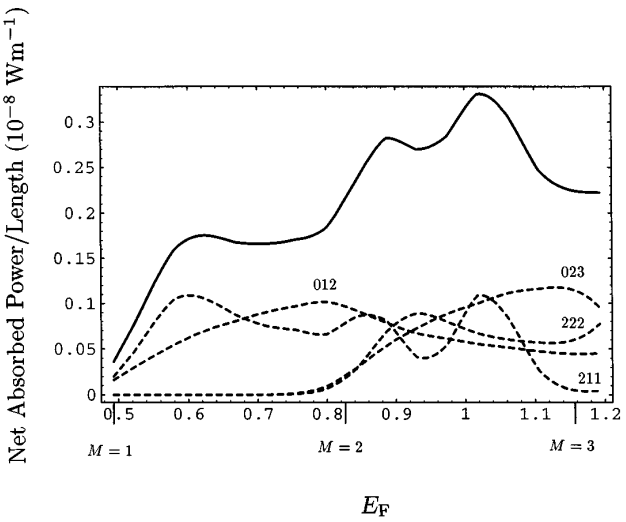

Figure 6. The net absorbed power per unit wire length versus E_F for $T_h = 8.8$ K, $T_e = T_a = 1.3$ K, heater dimensions $\Delta x \times \Delta y = 100\ \mu\text{m} \times 10\ \mu\text{m}$ and heater–wire distance $D = 380\ \mu$m. The locations of the subband edges are given. Also shown are the individual contributions from the dominant channels (dashed lines). The individual channels are labeled: sMN. For example, 012 stands for the absorption of a longitudinal phonon by an electron in the $M = 1$ subband, causing it to undergo a transition to the $N = 2$ subband. The complicated E_F dependences are a consequence of the peculiar effective heater geometry for FT phonons (figure 5).

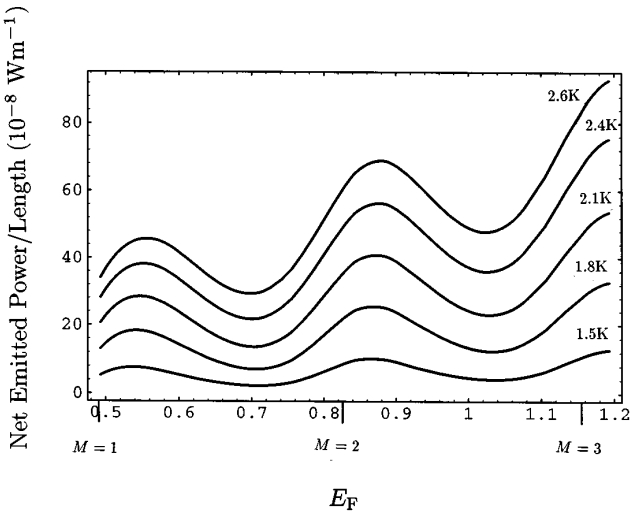

Figure 7. The net emitted power per unit wire length for $T_h = T_a = 1.3$ K and a selection of values $T_e > T_a$.

From figure 5, we see that this is not the case: because of the small Δy heater dimension-to-heater-wire distance ratio, most heater phonons do not have sufficient q_y wavevector components to be absorbed by the wire. There is clearly no such geometrical restriction for emission, however.

We can conceive of several possible explanations as to how the actual wire circumvents this obstruction to phonon absorption:

(i) *Disorder*. As discussed in section 2, the real wire is disordered. One consequence of disorder is to relax momentum conservation parallel to the wire for the process of absorption or emission of a phonon by an electron. Therefore, condition (17) does not have to be strictly satisfied. Disorder only affects the net absorbed power (11) provided $\overline{h}/\tau_M > k_B T_e$ [18]. For $T_e \sim 1$ K and $w \approx 20$ nm, this gives for the mean free path: $l_M < 0.5\ \mu\text{m} \ll L$.

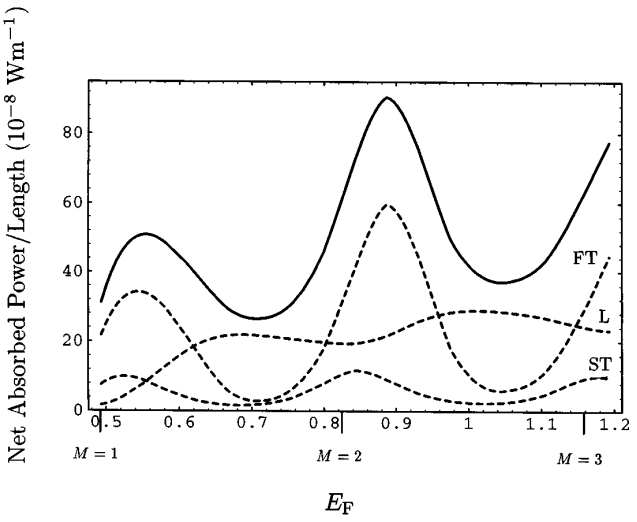

Figure 8. The net absorbed power per unit wire length versus E_F for $T_h = 8.8$ K, $T_e = T_a = 1.3$ K, heater dimensions $\Delta x \times \Delta y = 1500\ \mu\text{m} \times 150\ \mu\text{m}$ and heater–wire distance $D = 380\ \mu\text{m}$. The dashed lines give the individual phonon polarization contributions.

(ii) *Diffuse scattering.* In the experiment, the time interval between the onset of heater excitation and the instant at which the wire resistance is recorded just exceeds the heater–wire traverse time for transverse phonons. This is so as not to have a contribution from heater phonons which have reflected from the back surface (or sides) of the GaAs substrate. However, on the wire side of the substrate, the separation between the electron gas and the various interfaces, metal gates and substrate surface is of the order of nanometres. Therefore, the time resolution of the resistance measurement is not fine enough to exclude the contribution to the resistance change from heater phonons which have reflected from the surface/interfaces on the wire side. Non-specular reflection will increase the range of q_y wavevector components and thus such phonons may give a significant contribution to the measured resistance change. Figure 8 illustrates clearly the effect of increasing the q_y range on the E_F dependence of the net absorbed power; notice the sharp peaks at approximately the subband edges. Figure 9 gives the angular ranges; notice that condition (18) is now easily satisfied. Here, the increased q_y range is achieved by scaling up the dimensions of the heater. Non-specular reflection will have a similar effect on the absorbed power.

(iii) *Non-equilibrium electrons.* We have made the simplifying assumption that the electron gas is in thermal equilibrium during absorption of heater phonons. This requires that the electron–electron scattering rate be larger than the electron–phonon scattering rate for the considered heater temperatures. As was mentioned above, the electron–electron rate for a quantum wire depends strongly on the wire disorder. Therefore, without knowing the

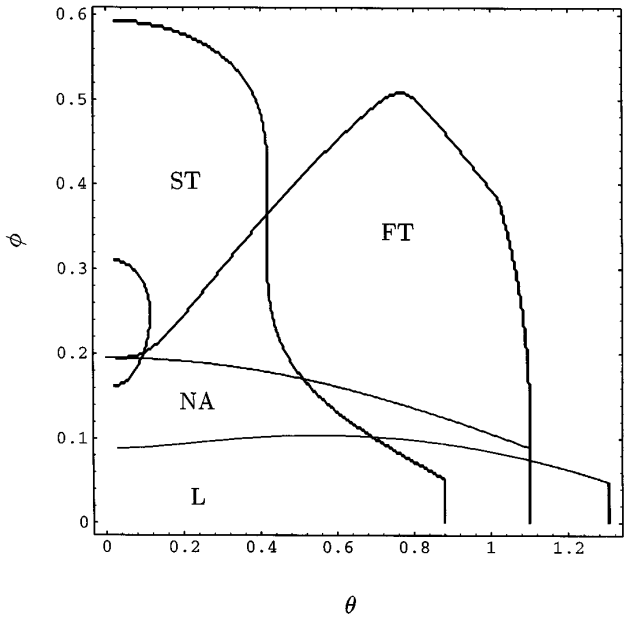

Figure 9. The boundaries of the phonon wavevector angular ranges for heater dimensions $\Delta x \times \Delta y = 1500\ \mu\text{m} \times 150\ \mu\text{m}$ and heater–wire distance $D = 380\ \mu\text{m}$.

disorder strength (i.e. impurity scattering rate), it is not possible to estimate the electron–electron rate for the wire used in the experiment. We can, however, estimate the change in electron distribution ignoring completely impurity and electron–electron scattering and compare the magnitude of this non-equilibrium change with that of the change obtained assuming equilibrium. Let $\delta f_M(k,t) = f_M(k,t) - f_0(E_M + k^2/2m_*)$ denote the (time-dependent) change in the electron distribution from the equilibrium distribution f_0 at the ambient temperature T_a. A straightforward application of kinetic theory gives approximately

$$\delta f_M(k,t) \approx \mathcal{T}(k) C_{\text{e-ph}}[f_0, \delta\rho]\left(1 - \text{e}^{-t/T(k)}\right) \tag{19}$$

where $\mathcal{T}(k) = Lm_*/\overline{h}k$ is the electron escape time from the wire† and we suppose the heater pulse reaches the wire at time $t = 0$. The electron–phonon collision integral term is (cf [19])

$$\begin{aligned} C_{\text{e-ph}}[f_0, \delta\rho] = \frac{2\pi}{\overline{h}} \sum_{N,s,\boldsymbol{q}} |M_{MNs}(\boldsymbol{q})|^2 \delta\rho_s(\boldsymbol{q},t) \\ \times \left\{ f_0\left(E_N + \overline{h}^2(k-q_y)^2/2m_*\right)\left[1 - f_0\left(E_M + \overline{h}^2k^2/2m_*\right)\right] \right. \\ \times \delta\left(E_M + \overline{h}^2k^2/2m_* - E_N - \overline{h}^2(k-q_y)^2/2m_* - \overline{h}\omega_s(\boldsymbol{q})\right) \\ - f_0\left(E_M + \overline{h}^2k^2/2m_*55\right)\left[1 - f_0\left(E_N + \overline{h}^2(k+q_y)^2/2m_*\right)\right] \\ \left. \times\ \delta\left(E_M + \overline{h}^2k^2/2m_* - E_N - \overline{h}^2(k+q_y)^2/2m_* + \overline{h}\omega_s(\boldsymbol{q})\right)\right\} \end{aligned} \tag{20}$$

where the change in phonon distribution from the ambient distribution is

$$\delta\rho_s(\boldsymbol{q},t) = \Theta(t)\Theta_s(\boldsymbol{q})\left[\left(\text{e}^{\overline{h}\omega_s(\boldsymbol{q})/k_\text{B}T_\text{h}} - 1\right)^{-1} - \left(\text{e}^{\overline{h}\omega_s(\boldsymbol{q})/k_\text{B}T_\text{a}} - 1\right)^{-1}\right]. \tag{21}$$

† I thank A Shik for pointing out the importance of the escape time.

For $k^{-1} \sim w = 20$ nm and $L = 10\ \mu$m, the escape time is $\mathcal{T} \sim 10^{-10}$ s, which is much less than the timescale of the resistance measurement (tens of nanoseconds) and hence we can neglect the exponential term in (19). Comparing the collision term (20) with the formula (11) for the net absorbed power, we obtain the following rough estimate for the magnitude of the distribution change when the electron energy is within $k_B T_e$ of E_F:

$$\frac{|\delta f|}{f_0} \sim \frac{\mathcal{T} P w}{k_B T_h} \sim 10^{-5} \tag{22}$$

where the net absorbed power is $P \sim 10^{-9}$ W m^{-1} (see figure 6) and $T_h \sim 10$ K. From (22), we see that the effective temperature increase will be much less than 1 K. Thus, even supposing a non-equilibrium electron distribution, the discrepancy remains. (Note, also, that including the energy loss due to electrons leaving the wire in the earlier analysis which assumed thermal equilibrium will lower even further the estimated electron temperature increase.)

(iv) *Weak localization with electron–phonon phase relaxation.* In contrast to the three mechanisms discussed in the present paper, weak localization with electron–phonon phase relaxation does not require a change in the electron distribution in order to produce a resistance decrease. This is because the electron–phonon phase relaxation rate depends directly on the non-equilibrium phonon distribution. In order to test this possibility, we must go beyond the qualitative analysis of reference [10] and estimate the weak localization contribution to the conductance. However, from equation (8) it is clear that such an estimate is only possible provided we know the backscattering length.

4. Conclusion

We have investigated the interaction between a non-equilibrium acoustic phonon beam and disordered quantum wire electron gas. In the experiment [1], it was found that such an interaction caused the wire conductance to increase and, furthermore, peaks in the conductance increase were observed at approximately the same gate voltage values as for the conductance step edges. We showed that such behaviour is a consequence of electron heating due to phonon absorption and the temperature dependence of either of the following two disorder scattering mechanisms: (i) impurity scattering in the presence of electron–electron interactions (figure 4), (ii) weak localization with phase relaxation governed by electron–electron scattering (equation (10)). The temperature dependence of Coulomb scattering from remote donor impurities was ruled out, because of the occurrence of E_F regions of negative conductance change (figure 3).

The estimated electron temperature increase (figures 6 and 7) was much lower than that found in the experiment. Because of the small size of the heater dimension parallel to the wire, most heater phonons directly incident on the wire do not have enough momentum component parallel to the wire in order to be absorbed by the electrons. One possible resolution given, is to include in the model the contribution from phonons which have reflected from the surface/interfaces closest to the wire. Non-specular reflection may result in an increase in angular range sufficient to overcome the stringent constraints which energy conservation and momentum conservation parallel to the wire place on absorption (figures 8 and 9).

In order to determine whether the conductance increase is due to electron–electron modified impurity scattering or to weak localization, it is essential that magnetoconductance measurements be carried out. Furthermore, the heater dimension parallel to the wire should be made much larger, say 100 μm instead of 10 μm, so as remove energy/momentum

conservation restrictions to the absorption of heater phonons directly incident on the wire. The measured and predicted electron temperature increases should then be compared to see if there is still a large discrepancy. Finally, using instead a laser beam focused onto a spot on a metal film deposited on the back surface of the substrate to produce a non-equilibrium phonon beam [20], we can explore more effectively the phonon momentum angular dependence of the electron–phonon interaction.

Acknowledgments

The author is grateful to K Benedict, A Kent, A Kozorezov, D Lehmann, A MacKinnon, A Naylor, A Shik and K Wigmore for helpful and stimulating conversations.

Appendix

We give here the derivation of the Drude + weak localization approximation to the wire conductance. A convenient starting point is the formulation of the conductance in terms of the advanced and retarded single electron Green functions [21]:

$$\begin{aligned} C = \frac{e^2\hbar^3}{8\pi m_*^2 L^2}\int_0^\infty \mathrm{d}E\,\frac{\partial}{\partial E}\left(\frac{1}{\mathrm{e}^{\beta(E-E_\mathrm{F})}+1}\right) \\ \times\int_{-\infty}^{+\infty}\mathrm{d}x\int_{-L/2}^{+L/2}\mathrm{d}y\int_{-\infty}^{+\infty}\mathrm{d}z\int_{-\infty}^{+\infty}\mathrm{d}x'\int_{-L/2}^{+L/2}\mathrm{d}y'\int_{-\infty}^{+\infty}\mathrm{d}z' \\ \Big[\overline{\partial^2_{yy'}(G^{(+)}(\boldsymbol{r},\boldsymbol{r}',E)-G^{(-)}(\boldsymbol{r},\boldsymbol{r}',E))(G^{(+)}(\boldsymbol{r}',\boldsymbol{r},E)-G^{(-)}(\boldsymbol{r}',\boldsymbol{r},E))} \\ +\overline{(G^{(+)}(\boldsymbol{r},\boldsymbol{r}',E)-G^{(-)}(\boldsymbol{r},\boldsymbol{r}',E))\partial^2_{yy'}(G^{(+)}(\boldsymbol{r}',\boldsymbol{r},E)-G^{(-)}(\boldsymbol{r}',\boldsymbol{r},E))} \\ -\overline{\partial_y(G^{(+)}(\boldsymbol{r},\boldsymbol{r}',E)-G^{(-)}(\boldsymbol{r},\boldsymbol{r}',E))\partial_{y'}(G^{(+)}(\boldsymbol{r}',\boldsymbol{r},E)-G^{(-)}(\boldsymbol{r}',\boldsymbol{r},E))} \\ -\overline{\partial_{y'}(G^{(+)}(\boldsymbol{r},\boldsymbol{r}',E)-G^{(-)}(\boldsymbol{r},\boldsymbol{r}',E))\partial_y(G^{(+)}(\boldsymbol{r}',\boldsymbol{r},E)-G^{(-)}(\boldsymbol{r}',\boldsymbol{r},E))}\Big] \end{aligned} \tag{23}$$

where m_* is the effective electron mass, L is the wire length and $\beta^{-1} := k_\mathrm{B}T_\mathrm{e}$, with T_e the electron temperature. The y-coordinate axis runs along the wire length, while the z-axis is normal to the 2DEG. The overlines denote averaging over an ensemble of random impurity distributions. In terms of the energy eigenfunctions $\phi_n(\boldsymbol{r})$ and eigenvalues E_n, the single electron retarded and advanced Green functions have the standard definitions:

$$G^{(\pm)}(\boldsymbol{r},\boldsymbol{r}',E) := \sum_n \frac{\phi_n(\boldsymbol{r})\phi_n^*(\boldsymbol{r}')}{E-E_n\pm\mathrm{i}\delta}. \tag{24}$$

Changing from the coordinate basis to the ideal wire energy eigenfunction basis $u_{M,k}(\boldsymbol{r}) := \Omega^{-1/3}\mathrm{e}^{\mathrm{i}ky}\chi_M(x)\psi_0(z)$, equation (23) becomes

$$\begin{aligned} C = \frac{2e^2\hbar^3}{\pi m_*^2\Omega^{2/3}L^2}\sum_k\frac{\sin^2(kL/2)}{k^2}\int_0^\infty\mathrm{d}E\,\frac{\partial f}{\partial E} \\ \times\sum_{M,g} g\left(K_{MM}^{(++)}(g,k,E)+K_{MM}^{(--)}(g,k,E)\right. \\ \left.-K_{MM}^{(+-)}(g,k,E)-K_{MM}^{(-+)}(g,k,E)\right) \end{aligned} \tag{25}$$

where Ω is a large normalizing volume, M denotes the transverse quantum number and K is defined as

$$K^{(ab)}_{MN}(g,k,E) := \sum_{J,s} s\overline{G^{(a)}_{MJ}\left(g+\tfrac{1}{2}k, s+\tfrac{1}{2}k\right) G^{(b)}_{NJ}\left(-g+\tfrac{1}{2}k, -s+\tfrac{1}{2}k\right)}. \tag{26}$$

The function K satisfies the following equation

$$K^{(ab)}_{MN}(g,k,E) \approx \overline{G}^{(a)}_{M}\left(g+\tfrac{1}{2}k\right)\overline{G}^{(b)}_{N}\left(g-\tfrac{1}{2}k\right) \times\left(g\delta_{MN} + \sum_{I,J,q} U_{MINJ}(q,E)K^{(ab)}_{IJ}(q-g,k,E)\right) \tag{27}$$

where U is the irreducible vertex function and

$$\overline{G}^{(\pm)}_{M}(k,E) = \left(E - E_M - \frac{\overline{h}^2k^2}{2m_*} \pm \mathrm{i}\frac{\overline{h}}{2\tau_M(k,E)}\right)^{-1}. \tag{28}$$

We have assumed here that $\overline{G}_{MN} \approx \overline{G}_M\delta_{MN}$. This requires that the ideal wire subband separation be much larger than the disorder broadening, i.e.

$$E_{M+1} - E_M \gg \frac{\overline{h}}{\tau_M}. \tag{29}$$

To lowest (i.e. quadratic) order in the single scatterer potential $V(\boldsymbol{r}) = \Omega^{-1}\sum_{\boldsymbol{q}} V(\boldsymbol{q})\exp(\mathrm{i}\boldsymbol{q}\cdot\boldsymbol{r})$, the irreducible vertex function is

$$U_{MINJ}(q,E) \approx T_{MINJ}(q) \tag{30}$$

where

$$T_{MINJ}(q) := \frac{\eta}{(2\pi)^2\Omega^{1/3}}\int_{-\infty}^{+\infty}\mathrm{d}q_x\int_{-\infty}^{+\infty}\mathrm{d}q_z|V(q_x,q,q_z)|^2|Z(q_z)|^2Q_{MI}(q_x)Q^*_{NJ}(q_x). \tag{31}$$

The constant η is the impurity concentration and the functions Z and Q are defined as follows

$$Z(q_z) := \int_{-\infty}^{+\infty}\mathrm{d}z\mathrm{e}^{\mathrm{i}q_zz}\psi^*_0(z)\psi_0(z) \tag{32}$$

$$Q_{MN}(q_x) := \int_{-\infty}^{+\infty}\mathrm{d}x\mathrm{e}^{\mathrm{i}q_xx}\chi^*_M(x)\chi_N(x). \tag{33}$$

If we make the simplifying assumption that the impurity potential is a delta function in position space, then T is independent of q and substituting the right-hand side of equation (27) into equation (25), we find that the T part drops out in the sums over g and k. The sums are then straightforward to perform and we obtain for the conductance [14]:

$$C_0 \approx -\frac{2e^2}{\pi\overline{h}}\int\mathrm{d}E\frac{\partial f}{\partial E}\sum_M\frac{l_M(E)}{L}\left\{1-\frac{l_M(E)}{L}\left[1-\exp\left(-\frac{L}{l_M(E)}\right)\right]\right\}. \tag{34}$$

The scattering length is

$$l_M(E) = \frac{\overline{h}k_M(E)}{m_*}\tau_M(E) \tag{35}$$

where

$$k_M(E) = \sqrt{\frac{2m_*}{\overline{h}^2}(E-E_M)} \tag{36}$$

is the wavenumber and

$$\tau_M^{-1}(E) \approx \frac{m_* \eta |V|^2}{2\pi^2 \bar{h}^3} \sum_N k_N^{-1}(E) \int \mathrm{d}q_x \mathrm{d}q_z |Z(q_z)|^2 |Q_{MN}(q_x)|^2 \tag{37}$$

is the scattering rate. The upper limit of the sum over the transverse quantum number M in (34) is set by the condition $E_M < E$. The upper limit for the sum in (37) is similarly set. The Born approximation (37) is valid provided $E - E_M \gg \bar{h}/\tau_M(E)$.

We now obtain the weak localization contribution to the wire conductance. The derivation outlined below is a straightforward generalization of the usual one for the single subband case (see, e.g., reference [7]). Suhrke and Wilke [22] also consider the multisubband case, but neglect the dependence of the scattering rate on the M-quantum number.

Let us again assume that we have a q-independent scattering potential and also that

$$l_M(E) \ll l_M^\phi(E) < L \tag{38}$$

where l_M^ϕ is the phase relaxation length, given in terms of the velocity $v_M := \bar{h}k_M/m_*$ and phase relaxation time τ_M^ϕ as

$$l_M^\phi = v_M \sqrt{\tau_M \tau_M^\phi}. \tag{39}$$

From equations (27) and (25), we obtain for the weak localization correction:

$$C_{\mathrm{wl}} \approx -\frac{e^2 \bar{h}^3}{\pi m_*^2 \Omega^{1/3} L} \int \mathrm{d}E \frac{\partial f}{\partial E} \sum_{M,g,q} g(q-g) G_M^{(+)}(g,E) G_M^{(-)}(g,E)$$
$$\times W_M(q,E) G_M^{(+)}(q-g,E) G_M^{(-)}(q-g,E) \tag{40}$$

where the overlines on the G's have been omitted. The function W denotes the sum over all 'fan' diagram contributions to the irreducible vertex function and is given by

$$W_M(q,E) = \sum_{I,J} T_{MI} \Pi_I(q,E) M_{IJ}(q,E) T_{JM} \tag{41}$$

where $T_{MN} := T_{MNMN}$ (see equation (31)),

$$\Pi_I(q,E) := \sum_k G_I^{(+)}(k,E) G_I^{(-)}(k-q,E) \tag{42}$$

and where M_{IJ} is the solution to the following equation

$$M_{IJ}(q,E) = \delta_{IJ} + \sum_K T_{IK} \Pi_K(q,E) M_{KJ}(q,E). \tag{43}$$

Performing the sum over g in (40), we obtain

$$C_{\mathrm{wl}} \approx \frac{e^2}{\pi \bar{h} L} \int \mathrm{d}E \frac{\partial f}{\partial E} \sum_{M,I,J} \tau_{MI}^{-1} \tau_I \left(\pi^{-1} \int \mathrm{d}q M_{IJ}(q) \right) \tau_{JM}^{-1} \tau_M^3 v_M^2 \tag{44}$$

where the upper limits of the transverse quantum number sums are set as in (34) and where τ_{MN}^{-1} denotes the individual scattering rate into the Nth subband, i.e.

$$\tau_M^{-1}(E) = \sum_N \tau_{MN}^{-1}(E). \tag{45}$$

Performing the sum over k in (42), with τ_M^{-1} replaced by $\tau_M^{-1} + \tau_M^{\phi -1}$ in (28), we obtain for M_{IJ}:

$$M_{IJ}^{-1}(q) \approx \delta_{IJ} - \tau_{IJ}^{-1} \tau_J \left(1 - \frac{\tau_J}{\tau_J^\phi} \right) + q^2 \tau_{IJ}^{-1} \tau_J^3 v_J^3. \tag{46}$$

The final steps are the inversion of (46) to obtain M_{IJ} and the q-integration in (44).

For the case where intersubband elastic scattering is negligible, i.e. $\tau_{IJ}^{-1} \approx \tau_I^{-1}\delta_{IJ}$, the matrix inversion is straightforward and we obtain

$$C_{\mathrm{wl}} \approx \frac{e^2}{\pi\hbar}\int \mathrm{d}E\,\frac{\partial f}{\partial E}\sum_M \frac{l_M^{\phi}(E)}{L}. \tag{47}$$

Suppose, in addition to condition (29), we also have $k_{\mathrm{B}}T_{\mathrm{e}} \ll E_{M+1} - E_M$ and that E_{F} is, say, somewhere in between (but not too close to) the $M = 1$ and $M = 2$ subband edges. Then for non-negligible intersubband scattering, i.e. $\tau_{IJ}^{-1} \sim \tau_I^{-1}$, we obtain from (46) and (44)

$$C_{\mathrm{wl}} \approx \frac{e^2}{\pi\hbar}\int \mathrm{d}E\,\frac{\partial f}{\partial E}L^{-1}\left(\frac{\tau_{10}^{-1}\tau_0 v_0^2 + \tau_{01}^{-1}\tau_1 v_1^2}{\tau_{10}^{-1}\tau_0^{\phi-1} + \tau_{01}^{-1}\tau_1^{\phi-1}}\right)^{1/2}. \tag{48}$$

For q-dependent scattering potential, the conductance calculations are considerably more involved. We assume that the above final expressions for C_0 (equation (34)) and C_{wl} (equations (47) and (48)) still apply, provided we replace the scattering rate (37) in these formulae with the transport or (equivalently) backscattering rate:

$$\tau_M^{\mathrm{b}-1}(E) \approx \frac{m_*\eta}{4\pi^2\hbar^3}\sum_N k_N^{-1}(E)\int \mathrm{d}q_x\mathrm{d}q_z|V(q_x, k_M + k_N, q_z)|^2|Z(q_z)|^2|Q_{MN}(q_x)|^2. \tag{49}$$

References

[1] Naylor A J, Strickland K R, Kent A J and Henini M 1995 *XI Int. Conf. on Electronic Properties of 2D Systems (Nottingham)* Workbook and Programme p 353
[2] Paalanen M A, Tsui D C, Gossard A C and Hwang J C M 1984 *Phys. Rev.* B **29** 6003
[3] Hirakawa K and Sakaki H 1986 *Phys. Rev.* B **33** 8291
[4] Fukuyama H, Kohno H and Shirasaki R 1993 *J. Phys. Soc. Japan.* **62** 1109
[5] Ogata M and Fukuyama H 1994 *Phys. Rev. Lett.* **73** 468
[6] Tarucha S, Honda T and Saku T 1995 *Solid State Commun.* **94** 413
[7] Bergmann G 1984 *Phys. Rep.* **107** 1
[8] Nixon J A and Davies J H 1990 *Phys. Rev.* B **41** 7929
[9] Sakaki H 1980 *Japan. J. Appl. Phys.* **19** L735
[10] Blencowe M P and Shik A Y in preparation
[11] Laux S E, Frank D J and Stern F 1988 *Surface Sci.* **196** 101
[12] Hirler F, Smoliner J, Gornik E, Weimann G and Schlapp W 1990 *Appl. Phys. Lett.* **57** 261
[13] Kumar A, Laux S E and Stern F 1989 *Appl. Phys. Lett.* **54** 1270
[14] Velický B, Špička V and Mašek J 1989 *Solid State Commun.* **72** 981
[15] Altshuler B L, Aronov A G and Khmelnitsky D E 1982 *J. Phys. C: Solid State Phys.* **15** 7367
[16] Benedict K A 1991 *J. Phys.: Condens. Matter* **3** 1279
[17] Shik A Y and Challis L J 1993 *Phys. Rev.* B **47** 2082
[18] Blencowe M P 1995 *Physica B* to appear
[19] Cantrell D G and Butcher P N 1987 *J. Phys. C: Solid State Phys.* **20** 1985
[20] Karl H, Dietsche W, Fisher A and Ploog K 1988 *Phys. Rev. Lett.* **61** 2360
[21] Fisher D S and Lee P A 1981 *Phys. Rev.* B **23** 6851
[22] Suhrke M and Wilke S 1992 *Phys. Rev.* B **46** 2400